





Article

Hybrid Krill Herd-ANN Model for Prediction Strength and Stiffness of Bolted Connections

Iman Faridmehr ¹, Mehdi Nikoo ², Mohammad Hajmohammadian Baghban ^{3,*} and Raffaele Pucinotti ⁴

¹ Institute of Architecture and Construction, South Ural State University, Lenin Prospect 76, 454080 Chelyabinsk, Russia; faridmekhri@susu.ru

² Young Researchers and Elite Club, Ahvaz Branch, Islamic Azad University, Ahvaz 61349-37333, Iran; m.nikoo@iauahvaz.ac.ir

³ Department of Manufacturing and Civil Engineering, Norwegian University of Science and Technology (NTNU), 2815 Gjøvik, Norway

⁴ Department of Mechanics and Materials, University of Reggio Calabria, 89124 Reggio Calabria, Italy; raffaele.pucinotti@unirc.it

* Correspondence: mohammad.baghban@ntnu.no

Abstract: The behavior of beam-to-column connections significantly influences the stability, strength, and stiffness of steel structures. This is particularly important in extreme non-elastic responses, i.e., earthquakes, and sudden column removal, as the fluctuation in strength and stiffness affects both supply and demand. Accordingly, it is essential to accurately estimate the strength and stiffness of connections in the analysis of and design procedures for steel structures. Beginning with the state-of-the-art, the capacity of three available component-based mechanical models to estimate the complex mechanical properties of top- and seat-angle connections with double-web angles (TSACWs), with variable parameters, were investigated. Subsequently, a novel hybrid krill herd algorithm-artificial neural network (KHA-ANN) model was proposed to acquire an informational model from the available experimental dataset. Using several statistical metrics, including the corresponding coefficient of variation (CoV), correlation coefficient (R), and the correlation coefficient provided by the Taylor diagram, this study revealed that the krill herd-ANN model achieved the most reliable predictive accuracy for the strength and stiffness of top- and seat-angle connections with double web angles.

Keywords: artificial neural network (ANN); beam-to-column joints; semi-rigid connections; component-based mechanical model; steel structures



Citation: Faridmehr, I.; Nikoo, M.; Baghban, M.H.; Pucinotti, R. Hybrid Krill Herd-ANN Model for Prediction Strength and Stiffness of Bolted Connections. *Buildings* **2021**, *11*, 229. <https://doi.org/10.3390/buildings11060229>

Academic Editor: Francisco López Almansa

Received: 17 April 2021

Accepted: 25 May 2021

Published: 27 May 2021

Publisher's Note: MDPI stays neutral with regard to jurisdictional claims in published maps and institutional affiliations.



Copyright: © 2021 by the authors. Licensee MDPI, Basel, Switzerland. This article is an open access article distributed under the terms and conditions of the Creative Commons Attribution (CC BY) license (<https://creativecommons.org/licenses/by/4.0/>).

1. Introduction

Steel beam-to-column connections are a fundamental component of steel structures, and their performance affects the overall structural behavior. Interest in utilizing bolted connections in steel constructions has significantly increased as a result of the uncertain and often inferior performance of welded connections during earthquakes [1–6]. According to Eurocode 3, Part 1–8, [7] a steel beam-to-column connection needs to have three essential characteristics: stiffness ($S_{j,ini}$), bending moment resistance ($M_{j,Rd}$), and plastic deformation capacity, ductility, or rotation capacity (φ_u). Generally, connections are subjected to complex loading and deformation interactions, and they serve as energy dissipation regions under extreme loading conditions. Experimental test results acknowledge that large variabilities are involved in the load-carrying capacity of welded steel beam-to-column connections. In fact, those variabilities are caused by different effects, such as [8]:

- Complex 3-D loading scenarios (axial loads, biaxial and shear, and torsional effects)
- Residual stresses as a result of welding, geometric imperfections, and strain hardening of column shear-panel zones, etc.
- Differences in weld quality and details (thickness, number of weld passes, and weld material)

- Post-weld treatment (removal, backing bar detail, heat treatment, and grinding)

After the 1994 Northridge and the 1995 Kobe earthquake, widespread analytical studies and experimental tests were commenced to examine the viability of using bolted connections in steel structures in high-seismicity zones [9–11]. A review of past literature shows that semi-rigid connections may be considered for seismic application where a large spectrum of such behavior positively influences structure strength and stability [12–14]. This research acknowledges that semi-rigid connections are characterized by reliable flexibility and appropriate rotational capacity.

Bolted top- and seat-angle connections without (TSACs) or with web angles (TSACWs) have been extensively used in steel and composite structures because of their relatively high moment capacity and easy construction. These types of connections are mainly designed to resist gravity loads of determinate steel beams. A schematic layout is proposed in Figure 1. The angles may be bolted or welded to the supported beam as well as to the supporting column. While the entire load is assumed to be transmitted to the column through the bottom seat angle, the top angle is considered mandatory for stability considerations. Traditionally, top- and seat-angle connections have been designed as shear connections, assuming negligible rotational resistance. However, the inherent flexural resistance of these connections should not be ignored when an accurate analysis of semi-rigid steel frames is desired [15,16].

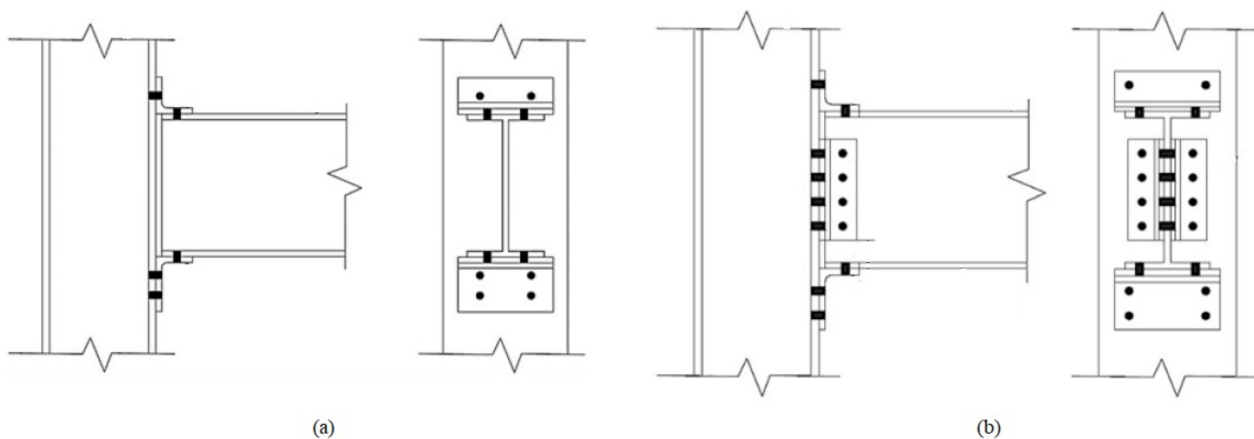


Figure 1. Reference configurations for (a) TSACs and (b) TSACWs.

Modeling the actual mechanical properties is of great importance in taking advantage of the flexible features of semi-rigid connections, leading to a reliable analysis and design. The majority of modeling methods are established based on mechanical theories considering geometric and material properties, hereafter called “mechanical” approaches. The main challenge in these methods is defining an acceptable number of components and conceptualization from physical behavior to analytical equations. Instead, informational methods have shown brilliant promise as alternatives to mechanical methods. Generally, in this approach, the connection behavior can be accurately represented by directly extracting a complex $M-\varphi$ curve relationship from the collected test data and subsequently analyzing it using a neural network or other optimization technique.

Over the past few years, a large number of studies have been performed in the area of modeling beam-to-column connections, from simplified global models to comprehensive finite element simulations [17–22]. Examples of simplified methods are analytical and empirical models where predictions will be made by determining key parameters (e.g., moment capacity, initial stiffness, etc.) and fitting a skeleton curve over these particular points [23]. In such an approach, the fundamental parameters can be extracted from experimental test data and represented with simple expressions, including polynomials, power functions, or a combination of these two expressions. In this model, the concern would be regarding the response of one component representative being the only basis of

the connection's flexibility. Once primary deformation sources are recognized, moment capacity and initial stiffness are calculated from geometric and material properties.

The component-based mechanical model was first introduced to simulate the overall performance of beam-to-column connections by taking into account the analytical models of the different flexibility sources (column shear panel zone, angles, etc.) and the non-linear constitutive relations of different components. Wales et al. [24] proposed the component-based method, and Tschemmerneegg et al. [25] developed this technique by using three groups of springs for bolted and welded connections. Madas et al. [26] investigated the application of the component-based analytical model by assembling different component contributions to predict the $M-\phi$ curve. In another study, De Stefano et al. [27] investigated the application of the component-based technique for double-web-angle connections, considering geometric and material properties. This study was extended by Shen et al. [28] to double-web-angle connections, taking into account slip effects and gap elements. Eurocode 3 [7] was the first design regulation to implement the component-based model concept to calculate the design parameters of bolted beam-to-column connections. Although the component-based method has the advantage of adapting to different connection types using the same principles, there is little discussion in Eurocode 3 about applying this method to other connections.

Even though the component-based mechanical model can predict virtually any $M-\phi$ curve, it is not possible to extend it beyond the calibration range. Moreover, it fails to predict considerably different behavior due to various failure modes when connections with different material properties and geometric are concerned. Generally, simplified models are suitable for application in frame analysis programs with design purposes. Instead, it is possible to represent each component contribution, along with complex interactions among the connection's components, by using detailed finite element models. A detailed finite element approach has high accuracy in simulating the complex $M-\phi$ curve of connections [29–32]. Nevertheless, this method is computationally intensive and time-consuming.

In this study, three different mechanical models proposed by Eurocode 3 [7], Kong and Kim [33], and Pucinotti [34] were presented, and their ability to accurately estimate initial stiffness $S_{j,ini}$, and the ultimate moment capacity M_n for TSACWs were examined and compared against each other, with the support of experimental data from the literature (77 specimens in total). Successively, a comprehensive ANN approach, combined with a metaheuristic krill herd algorithm (KHA), was developed to extract an informational model for TSACWs. Two statistical models, multiple linear regression and a genetic algorithm combined with an ANN model, were also developed to evaluate the accuracy of the proposed KHA-ANN model.

2. Databank Development

Having recognized that different parameters contribute to the ($M-\theta$) behavioral characterization of bolted beam-to-column connections, it is fundamental to first develop a consistent databank of test results for the examined connection typology. Experimental investigations and their results—when correctly extracted—notoriously allow for more robust and accurate classification of different behavioral features for beam-to-column connections, including $S_{j,ini}$, and M_n , but also hardening, non-linearities, progressive damage and degradation of mechanical parameters, rotation capacity, failure mechanism, and sequence. The same database is also strictly necessary for the development of the ANN model proposed herein.

In this paper, the preliminary verification of the component-based mechanical model for bolted TSACWs, as well as the training data to develop the ANN model, was carried out with the support of experimental data from the literature. Table 1 presents a summary of the significant geometrical and material properties for the examined TSACW connections. The complete data of TSACW specimens are available in [35–37].

Table 1. Geometrical and mechanical characteristics of selected TSACW specimens.

Test	Beam	Column	Size of Bolts (mm)	Top Cleat (mm)	Web Cleat (mm)	Yield Stress of Angle (N/mm ²)
8S1	H210 × 134 × 6.4 × 10.2	H310 × 254 × 9.1 × 16.3	19.1	L152 × 89 × 7.9	L102 × 89 × 6.4	285.4
8S2	H210 × 134 × 6.4 × 10.2	H310 × 254 × 9.1 × 16.3	19.1	L152 × 89 × 9.5	L102 × 89 × 6.4	285.4
8S3	H210 × 134 × 6.4 × 10.2	H310 × 254 × 9.1 × 16.3	19.1	L152 × 89 × 7.9	L102 × 89 × 6.4	285.4
8S4	H210 × 134 × 6.4 × 10.2	H310 × 254 × 9.1 × 16.3	19.1	L152 × 152 × 9.5	L102 × 89 × 6.4	285.4
8S5	H210 × 134 × 6.4 × 10.2	H310 × 254 × 9.1 × 16.3	19.1	L152 × 102 × 9.5	L102 × 89 × 6.4	285.4
8S6	H210 × 134 × 6.4 × 10.2	H310 × 254 × 9.1 × 16.3	19.1	L152 × 102 × 7.9	L102 × 89 × 6.4	285.4
8S7	H210 × 134 × 6.4 × 10.2	H310 × 254 × 9.1 × 16.3	19.1	L152 × 102 × 9.5	L102 × 89 × 6.4	285.4
8S8	H210 × 134 × 6.4 × 10.2	H310 × 254 × 9.1 × 16.3	22.2	L152 × 89 × 7.9	L102 × 89 × 6.4	277
8S9	H210 × 134 × 6.4 × 10.2	H310 × 254 × 9.1 × 16.3	22.2	L152 × 89 × 9.5	L102 × 89 × 6.4	277
8S10	H210 × 134 × 6.4 × 10.2	H310 × 254 × 9.1 × 16.3	22.2	L152 × 89 × 12.7	L102 × 89 × 6.4	277
14S1	H358 × 172 × 7.9 × 13.1	H323 × 310 × 14 × 22.9	19.1	L152 × 102 × 9.5	L102 × 89 × 6.4	285
14S2	H358 × 172 × 7.9 × 13.1	H323 × 310 × 14 × 22.9	19.1	L152 × 102 × 12.7	L102 × 89 × 6.4	365
14S3	H358 × 172 × 7.9 × 13.1	H323 × 310 × 14 × 22.9	19.1	L152 × 102 × 9.5	L102 × 89 × 6.4	285
14S4	H358 × 172 × 7.9 × 13.1	H323 × 310 × 14 × 22.9	19.1	L152 × 102 × 9.5	L102 × 89 × 9.5	285
14S5	H358 × 172 × 7.9 × 13.1	H323 × 310 × 14 × 22.9	19.1	L152 × 102 × 9.5	L102 × 89 × 6.4	277
14S6>	H358 × 172 × 7.9 × 13.1	H323 × 310 × 14 × 22.9	19.1	L152 × 102 × 12.7	L102 × 89 × 6.4	277
14S8	H358 × 172 × 7.9 × 13.1	H323 × 310 × 14 × 22.9	19.1	L152 × 102 × 15.9	L102 × 89 × 6.4	277
14S9	H358 × 172 × 7.9 × 13.1	H323 × 310 × 14 × 22.9	19.1	L152 × 102 × 12.7	L102 × 89 × 6.4	277

3. Component-Based Mechanical Methods

Previous experimental research on the $M-\varphi$ behavior of bolted-angle connections has revealed that the length in the vertical leg, the thickness of the top cleat, and the beam depth are the most critical features that affect connection and $M-\varphi$ behavior [10,38,39]. The component-based mechanical approach characterizes the $M-\varphi$ relationship through the superposition of the main components' contributions. All deformation sources are defined by a mathematical expression representative of individual connection components. Accordingly, it is crucial to classify all deformation sources and possible failure patterns. Then, the constitutive relationship of each deformation source is derived to identify its deformational properties. Finally, by considering compatibility and equilibrium, all components should assemble to achieve a reliable component-based model.

Generally, bolted beam-to-column connections have more deformation sources than welded, fully rigid connections due to different components. Bolting provides fewer restraints on column, beam, and connection components than welding, resulting in more flexibility. The angles are recognized to be a deformation potential for the semi-rigid connections, which affects overall connection behavior. Recent research [40–42] indicated that bolted beam-to-column connections exhibit complex behavioral features, leading to a more complicated response. Generally, the modeling method supposed to take into account among others: (i) flange cleat flexural effects at large displacements, (ii) high flexural and axial flexibility of bolts, (iii) strain hardening effects, and (iv) effect of the plastic hinge on the angle leg and beam flange.

Pucinotti [34] developed a simplified mechanical model for TSAC connections where the connection behavior is characterized by the flange cleat in flexural bending, bolt effects, and the effect of the unilateral contact between the column flange and top flange cleat. The fundamental deformation sources of top- and seat-angle connections are shown in Figure 2. In this simplified model, the joint is conceived as two rigid bars connected by two non-linear springs representing the axial response of angles. The two rigid bars AB and CD are representative of the column and the connected beam, respectively. The beam and column are supposed to be fully rigid, relative to the top angle. Considering Figure 2, AC is incorporated into the model to simulate the flexural response of the top cleat's outstanding leg, and a spring, BE , simulates the bolted effect.

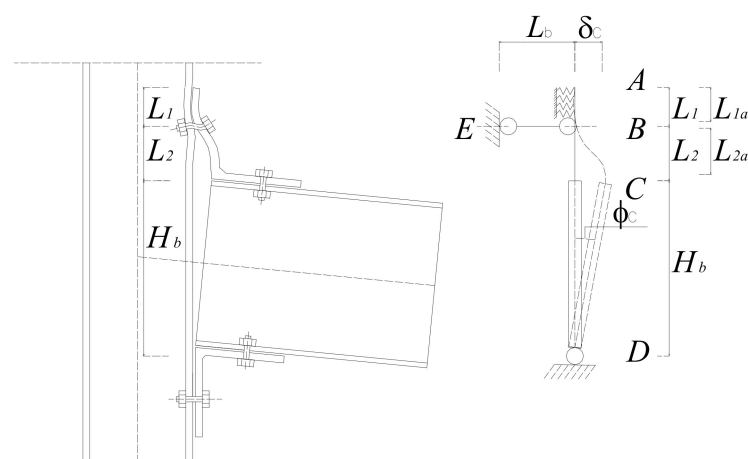


Figure 2. A simplified mechanical model of top- and seat-angle connections.

The AB part of the beam is schematized as an elastic beam supported by an assembly of elastic independent springs that represent the stiffness K_t of the column web [24]

$$K_t = \frac{t_{wc} E}{\ln(1 + H_c)} B_a \quad (1)$$

where t_{wc} = thickness of the web column; E = Young's modulus; H_c = height of the column; B_a = width of the outstanding leg.

The BC part of the top cleat is schematized as an inelastic beam with linear strain hardening, while the BE part is schematized as an elastic-perfectly-plastic spring. The end C of the outstanding leg is free to translate vertically, but it must rotate by $\varphi_c = \frac{\delta_c}{H_b}$, where δ_c is the vertical translation and H_b is the height of the connected beam. δ_c is calculated by applying the principle of virtual force from the mechanical model of Figure 2 as shown in the following equation

$$\delta_C = \int_0^{L_{2a}} M'(z)\chi(z)dz + N'_{BE} \frac{N_{BE}}{K_b} + M_B \frac{M_B}{K_\varphi} \quad (2)$$

where χ = curvature of the part BC of the top cleat, schematized as an inelastic beam; N'_{BE} = axial load; K_b = axial stiffness of the bolts = $\frac{E \pi d^2/4}{t_a+t_{fc}}$; t_a = thickness of the angle; t_{fc} = thickness of the flange column; K_φ = the rotational stiffness (as result of the top cleat and the stiffness Kt of the column web).

The mechanical model in the case of top- and seat-angle connections with web angles presents several additional components, in addition to top cleat deformation, equal to bolt rows of the web cleat, see Figure 3. The stiffness K_{tai} of the column web in correspondence to the i -th bolt row is provided by the formula [24]

$$K_{tai} = \frac{t_{wc}E}{\ln(1 + H_c)} B_{awi} \quad (3)$$

where t_{wc} = thickness of the web column; E = Young's modulus; H_c = height of the column; B_{awi} = width of the portion of the outstanding leg of the web angles.

The BC portion of the outstanding leg of the web cleat is schematized as an inelastic beam with linear strain hardening. The BE segment is conceptualized as an elastic-perfectly-plastic spring. The end C of the outstanding leg of the web cleat is free to translate horizontally, but its rotation $\varphi_{Cwi} = 0$. δ_{Cwi} is obtained by the application of the principle of virtual forces

$$\delta_{Cwi} = \int_0^{2L_{2awi}} M'(z)\chi(z)dz + N'_{BE} \frac{N_{BE}}{K_{bwi}} + M'_B \frac{M_B}{K_{\varphi wi}} \quad (4)$$

where χ = the curvature of the part BC of the beam; N'_{BE} = axial load; K_{bwi} = axial stiffness of the bolt $i = \frac{E \pi d^2/4}{t_{aw}+t_{fc}}$; t_{aw} = thickness of the web angle; t_{fc} = thickness of the flange column; $K_{\varphi wi}$ = rotational stiffness; L_{bwi} = the length of bolt i .

Kong and Kim [33] have used curve-fitting software to obtain the effects of top and seat angles on the $S_{j,ini}$ value of TSACWs; they developed a semi-empirical equation as follows:

$$S_{j,ini} = \frac{0.49El_t t_3^t \left(d + \frac{t_t}{2} + \frac{t_s}{2} + 2k_t \right) t_{cf} t_{bw}}{\left(g_t - t_t - \frac{d_b}{2} \right)^2} \left(\frac{d}{t_t} \right)^{0.3} + \frac{0.312n\alpha El_p^2 t_a}{(1+v)g_c} \quad (5)$$

In Equation (5), E is Young's modulus; l_t is the length of the top angle; t_t is the top angle thickness; t_s is the thickness of the seat angle; d is the height of the beam; k_t is the fillet size of the top angle; t_{cf} is the thickness of the column flange; t_{bw} is the thickness of the beam web; g_t is the distance from the top angle heel to the center of the bolts; d_b is the diameter of the bolts; n is the number of bolts; $\alpha = 1.0$ mm; l_p is the angle length of the web; t_a is the angle thickness of the web; v is Poisson's ratio; $g_c = g_1 - t_a$, as shown in Figure 4.

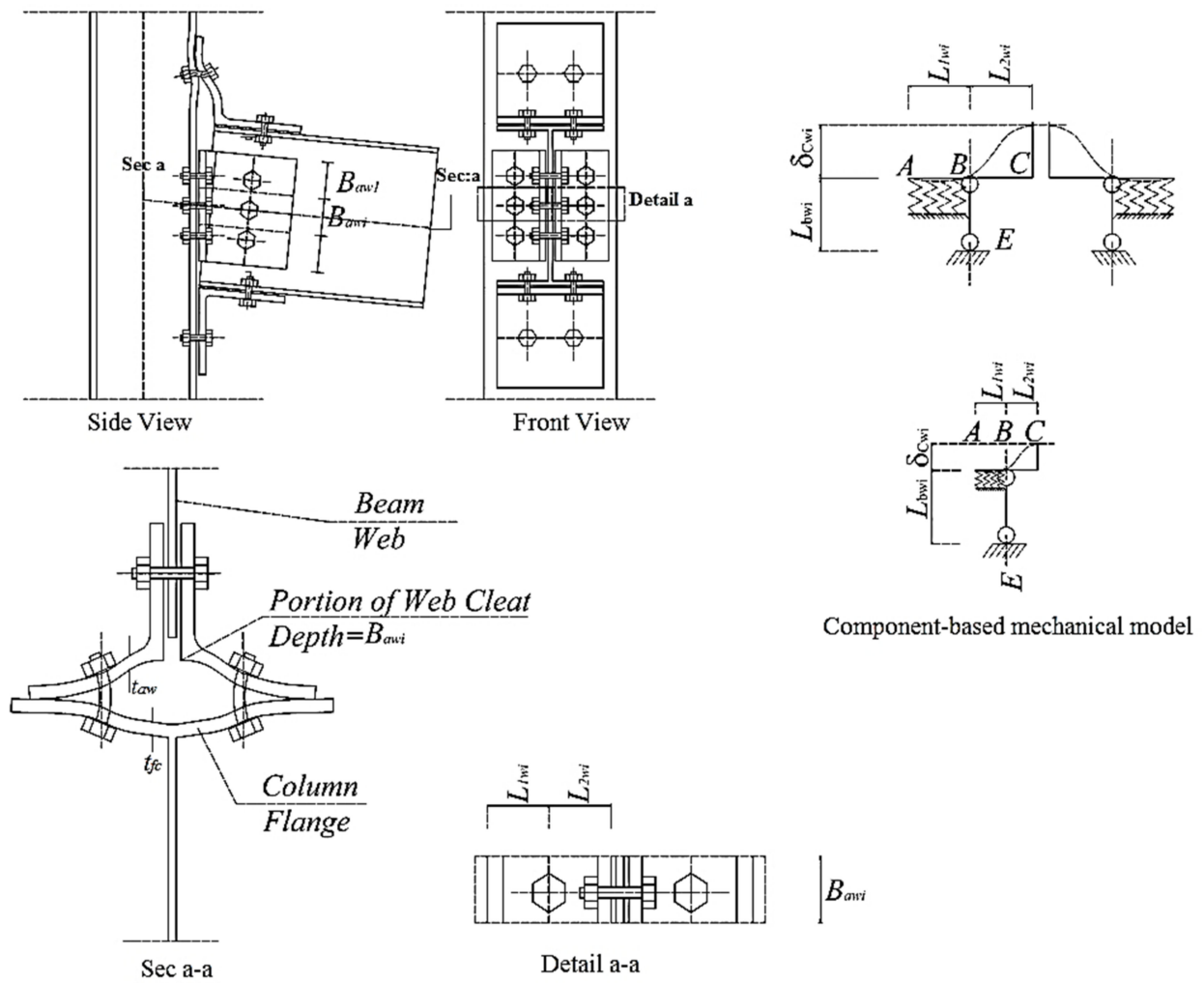


Figure 3. Mechanical model for top- and seat-angle connections with web angles.

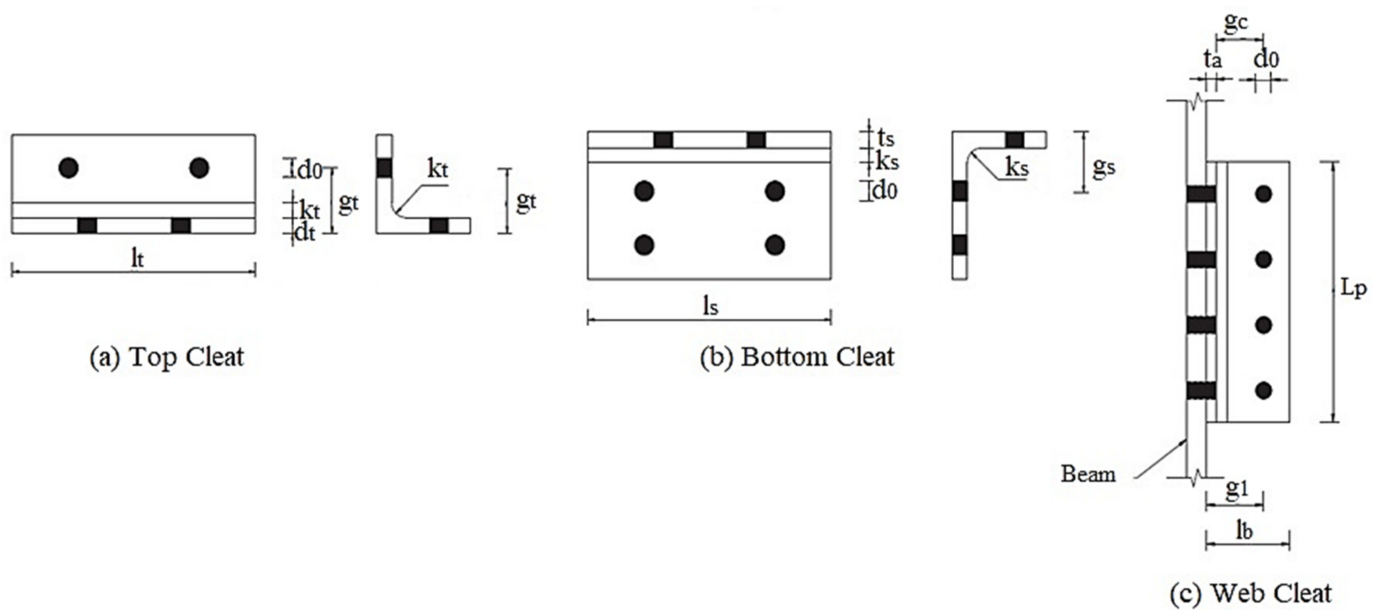


Figure 4. Parameters of TSACW connection.

For a TSAC with a single web cleat, Kishi and Chen [43] elaborated a model proposal for the detection of the collapse mechanism in 1990. Kong and Kim [33] extended the model and presented the following equation for estimating the ultimate moment capacity M_n of TSACW connections:

$$M_n^{top-seat} = M_{os} + M_p + V_{pt}d_2 + V_{pa}d_4 \quad (6)$$

In Equation (6), M_{os} is the plastic moment capacity of the seat angle; M_p is the plastic moment capacity of the top angle; V_{pt} is the ultimate shear force acting on the top angle; d_2 is a parameter related to the depth of the beam and the thickness of top and seat cleats; V_{pa} is a parameter that depends on the ultimate shear force at the upper and lower edges of the web cleat; d_4 is the distance between the plastic shear at the lower edge of the web cleat and the center of compression. These parameters are schematized in Figure 5.

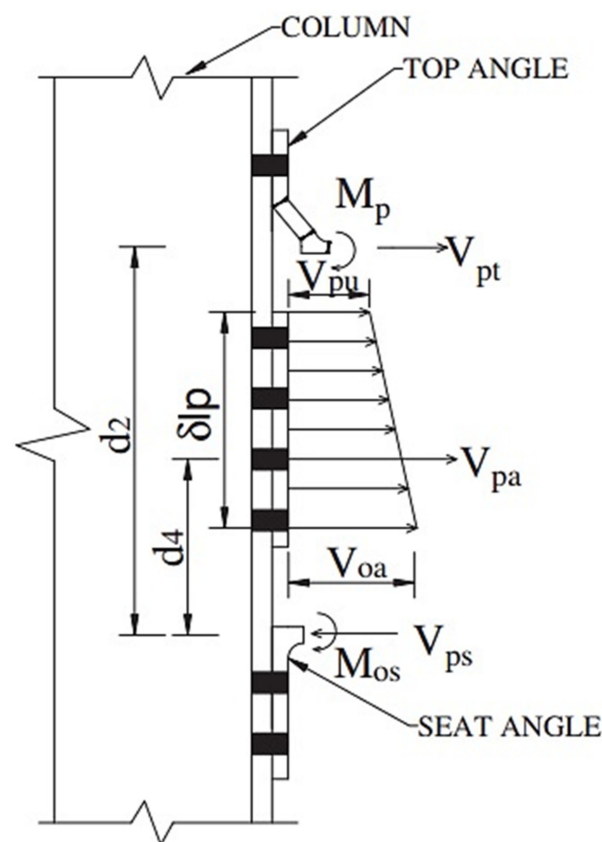


Figure 5. Collapse mechanism for TSACW.

Eurocode 3 [29] implemented a component method to estimate the $S_{j,ini}$ of TSACs. In this method, the connection behavior is simulated by a series of different components, each representative of an elastic spring with a specific stiffness and strength. It is possible to calculate the overall stiffness by assembling these springs in a parallel-series configuration, as shown in Figure 6.

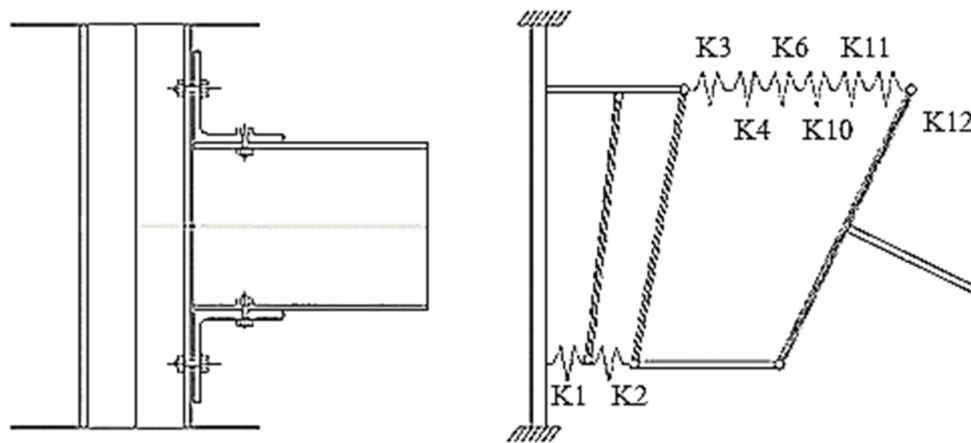


Figure 6. Modeling of TSAC connection recommended by Eurocode 3.

In Eurocode 3, the following components consider the stiffness coefficients of the column shear panel zone (K_1), the column flange in tension (K_3), the column flange in compression (K_2), flexural stiffness of the column flange (K_4), top cleat flexural stiffness (K_6), tensile stiffness of the bolts (K_{10}), and, for non-preloaded bolts, their shear stiffness (K_{11}) and their bearing stiffness (K_{12}). Therefore $S_{j,ini}$ of the TSAC is provided by

$$S_{j,ini} = \frac{Ez^2}{\sum_{i=1}^n 1/K_i} \quad (7)$$

where E is Young's modulus, z is the lever arm, K_i is the i -th component stiffness coefficient, and n is the number of joint components. Z should be taken as the distance from the bolt row in tension and the mid thickness of the leg of the seat cleat on the compression flange. The Eurocode 3 does not include a mechanical model for the TSACW connection. Accordingly, an extension of Eurocode 3 for TSACWs is proposed in this study by the authors [44]. For a bolt row in a web cleat, the stiffness illustrated in Figure 7 should be considered.

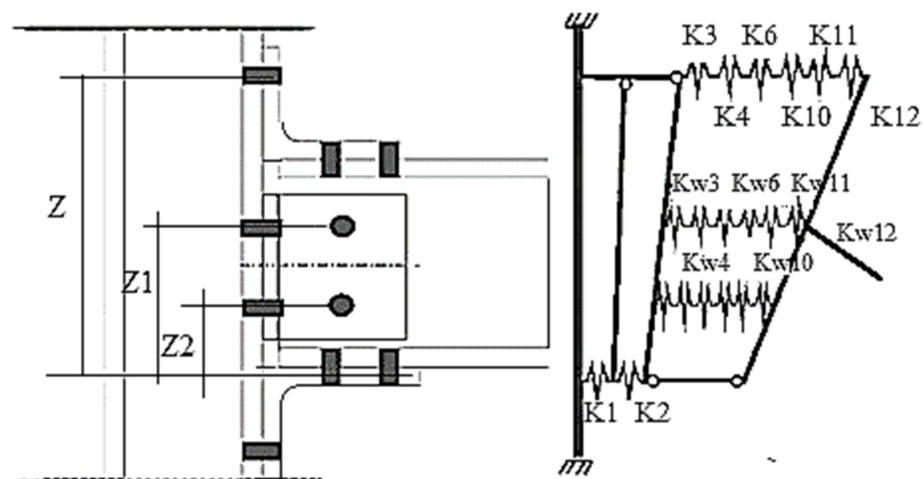


Figure 7. Eurocode 3 extension for TSACW connection.

The overall stiffness of basic components illustrated in Figure 7 is represented by a single equivalent stiffness coefficient k_{eq} calculated from the following equation

$$k_{eq} = \frac{S_{j,ini}}{Ez} + \frac{\sum k_{eff,r} z_r}{z_{eq}} \quad (8)$$

where $S_{j,ini}$ is the initial stiffness for TSAC and z_r is the distance between the center of compression cleat and bolt row r of the web cleat. Additionally,

$$k_{eff,r} = \frac{1}{\sum_i 1/k_{i,r}} \quad (9)$$

where $k_{i,r}$ is the stiffness coefficient representing component i relative to bolt row r , and

$$z_{eq} = \frac{\frac{S_{j,ini}}{E} + \sum_r k_{eff,r} z_r^2}{\frac{S_{j,ini}}{Ez} + \sum_r k_{eff,r} z_r} \quad (10)$$

Finally, the initial stiffness of TSACW can be calculated from the following equation

$$S_{j,ini} = \frac{Ez_{eq}}{k_{eq}} \quad (11)$$

In 2005, Eurocode 3 [7] propose an equation to estimate the M_n of TSAC and TSACW connections

$$M_n = F_{Rd}Z \quad (12)$$

where the Z is the lever arm and F_{Rd} is the design resistance of weak joint components, which can be one of the following: the top cleat in bending ($F_{tc,Rd}$), the bolts in tension, the beam flange in tension and compression, and the beam web in tension.

4. Informational Approach

An informational-based method is recognized as an alternative method to simulate complex structural and material behaviors that are not simply estimated by conventional methods. This alternative method simulates the behaviors via the information contained in the tested specimens. Accordingly, this is an important evolution from mathematical equations to preserve data that contain the necessary information on mechanical characteristics. In this approach, the underlying mechanics information is extracted from the experimental test data and processed in the neural network's program. Subsequently, the trained networks can be employed in the simulation process. Several researchers have applied neural networks to describe the complex behavior of different materials [45–47]. The application of neural networks to predict the $M-\theta$ curve of top and seat connections and end-plate connections has been investigated by [48–52].

ANNs are mathematical models inspired by biological neural systems. The neural networks determine the outputs based on the model inputs through processing units called neurons. One of the most common types of neural networks is the feedforward network, in which neurons are placed in layers that include an input layer, one or more hidden layers, and an output layer. In each layer, the neurons are entirely connected, and the net input of a neuron is always the sum of the weighted outputs from all neurons in the previous layer. Each neuron uses a function called the activation function for its net input to determine its output [53,54]. To connect the nodes in each layer, a parameter called "weight" is used. All weights of an ANN are usually adjusted randomly as a default condition; consequently, network outputs will have an associated error. To minimize the output error, the optimal ANN weight should be determined using the training data. This optimization process is called training the network [55].

4.1. Krill Herd Algorithm

The KHA is an intelligent group algorithm for optimization in engineering disciplines [56]. This algorithm has been used to achieve more efficiency in civil engineering by referring to a novel metaheuristic algorithm to determine the weight optimization of each ANN model. In this algorithm, krill individuals search for food in different places and are presented as different decision variables. The objective is to calculate the distance

between krill individuals and extra food availability, related to the cost. Therefore, the time-dependent position of a krill individual is measured by functional processes, which include the process of foraging, the search displacement, and the physical random diffusion [56–58]. Figure 8 shows a basic representation of the KHA.

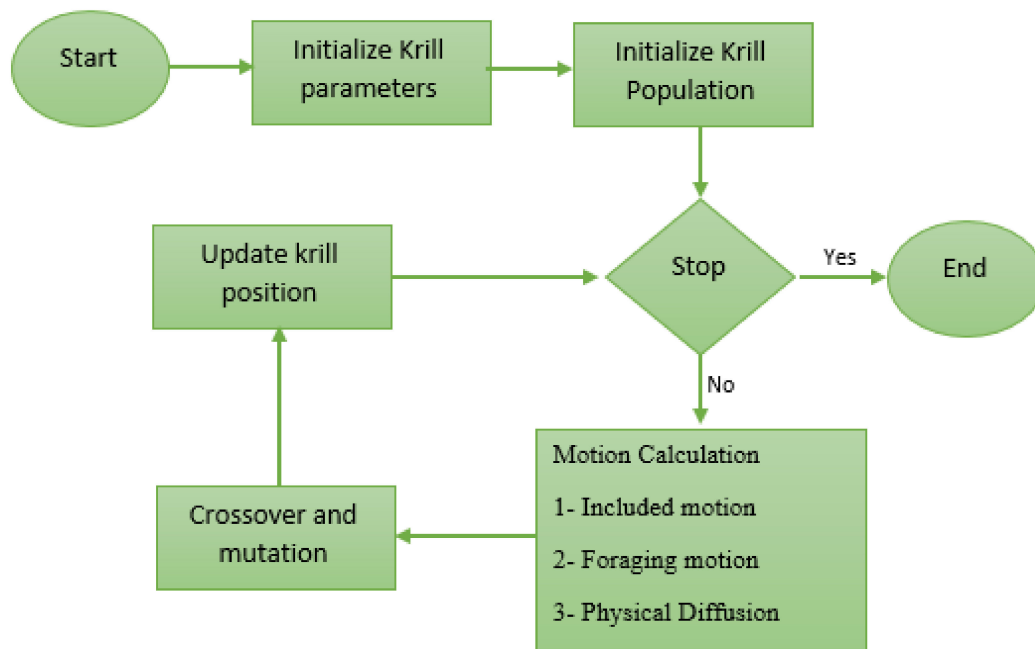


Figure 8. A flowchart of the krill herd optimization algorithm.

In the process of the foraging motion, the krill individual's velocity is always affected by another krill's displacement in the multidimensional search space, where the velocity changes dramatically and dynamically based on the internal influence parameters, including the influence of the target group and the repulsive effect. The displacement description of a krill individual can be formulated by Equations (13)–(18) [57].

$$\theta_i^{new} = \epsilon_i \theta_i^{max} + \mu_n \theta_i^{old} \quad (13)$$

$$\epsilon_i = \epsilon_i^{local} + \epsilon_i^{target} \quad (14)$$

$$\epsilon_i^{local} = \sum_{i=0}^{Ns-1} f_{ij} x_{ij} \quad (15)$$

$$f_{ij} = \frac{f_i - f_j}{f_w - f_b} \quad (16)$$

$$x_{ij} = \frac{x_i - x_j}{|f_w - f_b| rand(0.1)} \quad (17)$$

$$\epsilon_i^{target} = 2(rand(0.1) + \frac{i}{i_{max}}) f_i^{best} x_i^{best} \quad (18)$$

In these equations, θ_i^{max} represents the highest motion created and θ_i^{old} is the motion created. μ_n represents the algebraic magnitude of the motion created, while the target effects are shown by ϵ_i^{local} and ϵ_i^{target} . f_w and f_b are the worst and best population positions, respectively. f_i and f_j are the i th and j th krill individual proportions. The current number and the highest number are provided by i_{max} . To identify the neighboring members of

each krill individual, a sensor distance parameter (SD_i) was used (as shown in Figure 9), following equation [57]

$$SD_i = \frac{1}{5n_p} \sum_{i=0}^{n_p-1} |x_i - x_j| \quad (19)$$

where n_p represents the number of krill individuals in the population, while x_i and x_j represent the position of i th and j th krill, respectively [57].

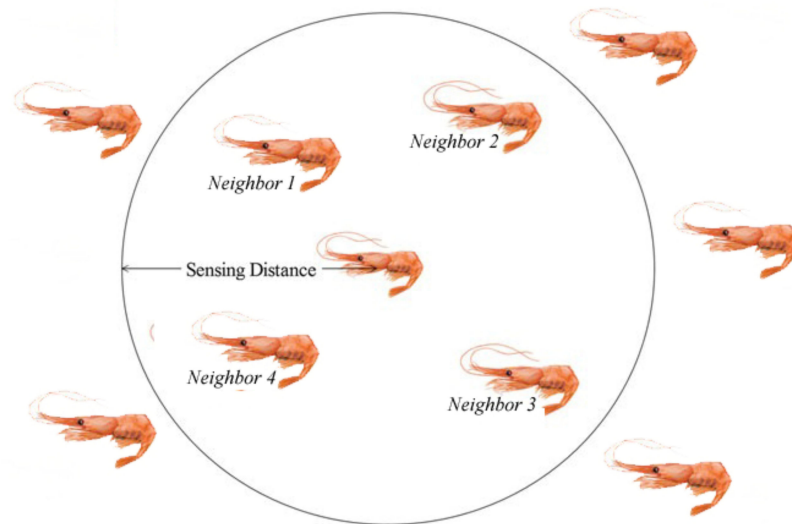


Figure 9. Sensing distance around an individual krill.

4.2. Training the KHA-ANN Model

To train the ANN for estimating two outputs of $S_{j,ini}$ and $(M_n/M_{p,beam})$, a total number of 77 specimens from references [36,37] were considered. Up to 80% of selected samples (62) were used for training, while the 20% portion (15 specimens) was used to test the network. Several variables, including the ratio of moment inertia from column to connected beam, the thickness of the top and bottom flange cleat, the maximum thickness of the right or left web cleat, bolt size, and the ratio of F_y column to F_y beam, were introduced as the input parameters. The input and output, as well as their properties, are shown in Table 2. Figure 10 also shows the correlation matrix of the input variables.

Table 2. Statistical parameters of input and output parameters.

Parameter	Type	Max	Min	Average	STD
Ratio of moment inertia of column/beam	Input	20.00	0.30	2.60	3.96
Thickness of top flange cleat (mm)	Input	15.90	0.00	8.11	4.79
Thickness of bottom flange cleat (mm)	Input	15.90	0.00	8.70	4.46
Max thickness of right/left web cleat (mm)	Input	15.00	0.00	6.17	4.51
bolt size (mm)	Input	24.00	16.00	19.51	1.70
Ratio of F_y column/ F_y beam	Input	1.13	0.80	1.00	0.09
$S_{j,ini}$ (kNm/rad)	Output	36,365.00	1633.00	12,021.75	9108.08
$M_n/M_{p,beam}$	Output	0.95	0.13	0.43	0.20

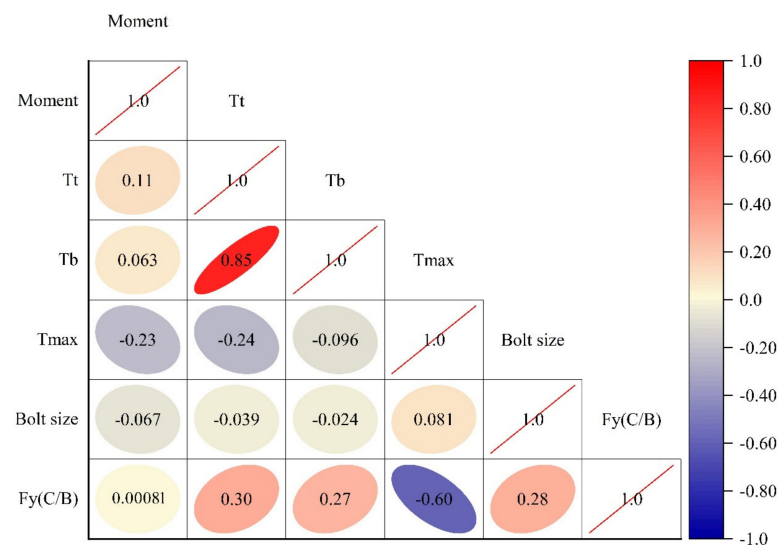


Figure 10. Correlation matrix of the input variables.

The histogram graphs of the studied output parameters ($S_{j,ini}$ and M_n/M_p beam) indicate that they follow a normal distribution, as depicted in Figure 11.

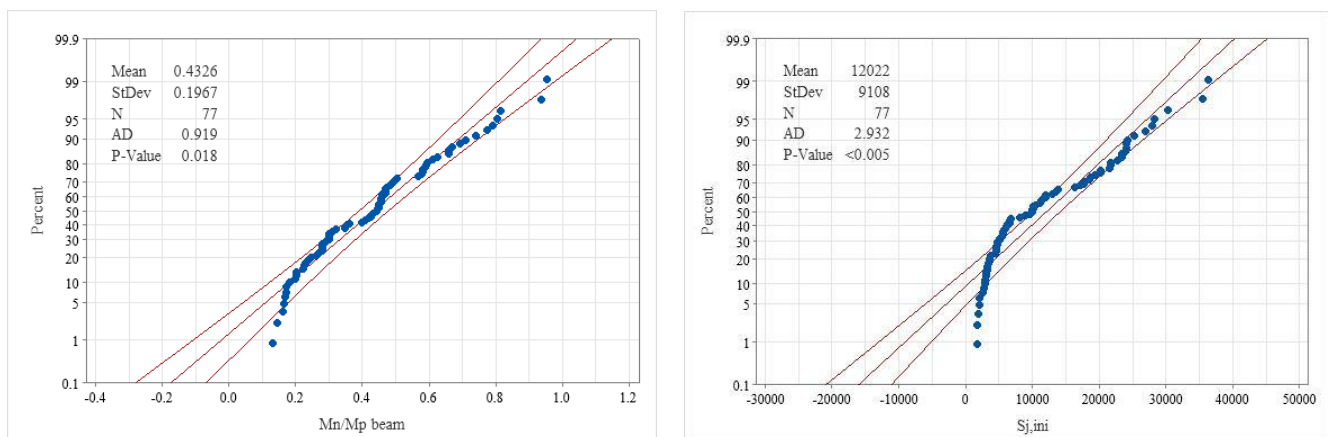


Figure 11. Histogram graphs of $S_{j,ini}$ and $\frac{M_n}{M_{p,beam}}$.

The number of hidden layers and the total number of neurons in the hidden layers in an ANN depends on the problem's nature [50]. Generally, the trial-and-error method is used to obtain the ideal architecture, which best reflects laboratory data characteristics. In this research, an innovative method for calculating the number of neurons in hidden layers is taken into account, namely

$$N_H \leq 2N_I + 1 \quad (20)$$

where N_H represents the number of neurons in the hidden layers and N_I is the number of input variables.

Since the number of influential input variables for the current study is equal to 6, the empirical Equation (20) shows that the number of neurons in hidden layers can be less than 13. Therefore, several networks with different topologies (with a maximum of 2 hidden layers and a maximum of 13 neurons) were trained and studied in this paper.

The hyperbolic tangent stimulation function and Levenberg–Marquardt training algorithm were used in all networks. The statistical indices used to evaluate the performance

of different topologies are the age absolute error (*AAE*), variance account factor (*VAF*), and model efficiency (*EF*) that are defined as follows [51]

$$EF = 1 - \frac{\sum_{i=1}^n (P_i - O_i)^2}{\sum_{i=1}^n (\bar{O}_i - O_i)^2} \quad (21)$$

$$VAF = \left[1 - \frac{var(O_i - P_i)}{var(O_i)} \right] \quad (22)$$

$$AAE = \frac{\left| \sum_{i=1}^n \frac{(O_i - P_i)}{O_i} \right|}{n} \times 100 \quad (23)$$

where p_i is the prediction of specimen i and o_i is the observation of specimen i .

After examining the different topologies of the networks, it was found that the lowest value of error characterizes the network with a 6-7-6-1 topology in *EF*, *VAF*, and *AAE*, and by the highest value of R^2 to estimate the two output parameters $S_{j,ini}$ and $(M_n/M_{p,beam})$, as shown in Table 3. It is necessary to mention that the error criteria for training and testing the selected data are calculated in the main range of variables and not in the normal range.

Table 3. Statistical results from the ANN model to determine the $S_{j,ini}$ and $\frac{M_n}{M_{p,beam}}$.

Type	Statistical Index	$S_{j,ini}$ (kNm/rad)	$M_n/M_{p,beam}$
Train	AAE	0.260	0.107
	EF	0.903	0.877
	VAF%	90%	88%
Test	AAE	0.085	0.095
	EF	0.993	0.890
	VAF%	99%	75%
All	AAE	0.226	0.104
	EF	0.920	0.880
	VAF%	92%	88%

In this study, as in for several structural engineering practice applications, the KHA was used as a new metaheuristic algorithm to determine the weight optimization of each ANN model, given that the $(M_n/M_{p,beam})$ output has a numerical range of 0–1 while the $S_{j,ini}$ output is characterized by a numerical range of 1600–37,000 (kNm/rad). This means that there is a big difference between the two target outputs. For modulation, two separate ANNs were hence used in this study, each one with one output. Their essential characteristics are summarized in Table 4.

Table 4. Feedforward ANN structure and topology.

No	Name	Features of Neural Network						
		Number of Input	Number of Output	Neural Network	Hidden Layer	Node	Learning Role	Transfer Function
2	KHA-ANN-M	6	1	Feedforward	2	7-6	Levenberg–Marquardt	Tansig
3	KHA-ANN-S	6	1	Feedforward	2	7-6	Levenberg–Marquardt	Tansig

M stands for the ultimate moment capacity of connections ($M_n/M_{p,beam}$); S stands for the initial stiffness of connections ($S_{j,ini}$).

Figure 12 shows the optimal topology of a feedforward network with two hidden layers, six input variables (neurons), and one output parameter.

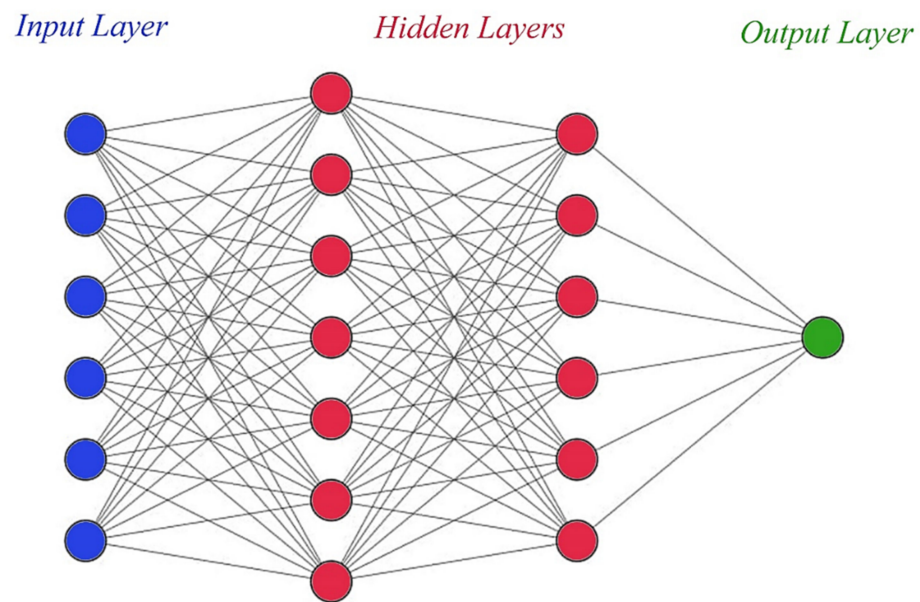


Figure 12. Optimized feedforward ANN with 6-7-6-1 structure.

The KHA has also been used to provide the least prediction error for the trained structure to optimize the weights and biases of the ANN model. The KHA parameters are also presented in Table 5.

Table 5. Features of KHA in feedforward ANN models.

No.	Name	Features of KHA					
		Number of Krills	Minimum Number of Krill Herd	Maximum Iteration	Maximum Induced Speed	D Max	
1	KHA-ANN-MS	KHA-Model 1	10	2	200	0.01	0.005
2	KHA-ANN-M	KHA-Model 2	5	2	200	0.01	0.005
3	KHA-ANN-S	KHA-Model 3	5	2	100	0.01	0.004

M stands for the ultimate moment capacity of connections ($M_n/M_{p,beam}$); S stands for the initial stiffness of connections ($S_{j,ini}$).

Features of the KHA, shown in Table 5, are defined as follows:

- I. Number of krill: the required number of krill for starting the optimization;
- II. Minimum number of krill herd: the minimum number of required krill in each group;
- III. Maximum iteration: maximum interaction between krill in one group or one group with another group;
- IV. Maximum induced speed: maximum induced speed between the two groups;
- V. D max: maximum radius in each group.

4.3. Multiple Linear Regression and Genetic Algorithm

Multiple linear regression and genetic algorithm models were also developed to validate the feedforward KHA-ANN model's accuracy in this study. In multiple linear regression, two or more independent variables have a significant effect on the dependent variable, as shown in Equation (16) [59]:

$$y = f(x_1, x_2, \dots) \rightarrow y = a_0 + a_1x_1 + a_2x_2 + \dots \quad (24)$$

In the above equation, y is the dependent variable; x_1, x_2, \dots are the independent variables; a_1, a_2, a_3, \dots are the coefficients of the regression equation. For input and output variables, different models of linear regression were investigated using MINITAB version 14.0 software. The following equations show multiple linear regression models for $S_{j,ini}$ and M_n/M_p outputs.

$$S_{j,ini} = 4526 - (630 \times I_{col}/I_b) + (889 \times th_{tc}) + (304 \times th_{bc}) - (285 \times Max - th_{wc}) + (1282 \times d_b)(24,013 \times fy_c/fy_b) \quad (25)$$

$$M_n/M_p = 1.004 - (0.00527 \times I_{col}/I_b) + (0.03663 \times th_{tc}) - (0.0103 \times th_{bc}) + (0.00346 \times Max - th_{wc}) - (0.0006 \times d_b) - (0.777 \times fy_c/fy_b) \quad (26)$$

For another evaluation of the KHA-ANN model, the genetic algorithm combined with ANNs was considered. The features of the genetic algorithm are shown in Table 6.

Table 6. Features of genetic algorithm in ANN models.

Parameter Name	Value
Selection mode	3
Population size	150
Maximum generations	250
Recommendation percentage	0.15
Cross percentage	0.15
Mutation percentage	0.7

5. Accuracy of Proposed KHA-ANN-Model

Tables 7 and 8 show the comparison between different models with experimental data for estimating $S_{j,ini}$ and M_n , respectively. Concerning the calculated average “Avg.” and standard deviation “STD” values, the results in Tables 7 and 8 indicate that the KHA-ANN model provides more reliable predictions for both $S_{j,ini}$ and M_n , compared to the Eurocode 3 [7], Kong and Kim [33], Pucinotti [34], multiple linear regression, and genetic algorithm formulations described earlier. Using the existing empirical models, $S_{j,ini}$ and M_n were either underestimated or overestimated however, the KHA-ANN predictions, conversely, was rely on underlying mechanism and characterized by minimum deviation.

Figures 13 and 14 show the scatter graph that provided the relationship between test results and the proposed KHA-ANN model for estimating the $S_{j,ini}$ and M_n parameters, respectively, compared to the mechanical and other informational models. The comparative results indicate that the KHA-ANN model offers a more reliable prediction for both the examined mechanical parameters, thus confirming the proposed model’s high potential and accuracy.

Table 7. Comparison of different models with literature test data, as obtained in terms of $S_{j,ini}$.

Test	$S_{j,ini}$ (kN·m/rad)	Test/EC3	Test/Kong and Kim	Test/ Pucinotti	Test/ KHA-ANN	Test/ Multiple Linear Regression	Test/ Genetic Algorithm
8S1	6000	0.62	0.81	1.09	1.07	0.70	0.82
8S2	13,846	0.44	1.49	1.21	1.10	1.31	1.45
8S3	10,099	0.49	1.03	1.35	1.15	1.17	1.39
8S4	1633	1.32	1.34	0.83	1.19	0.16	0.17
8S5	8089	1.65	1.26	1.07	1.08	0.77	0.85
8S6	4490	1.80	1.13	0.79	1.20	0.52	0.62
8S7	4638	1.17	0.96	1.24	1.22	0.44	0.48
8S8	6060	1.50	1.43	1.41	1.35	1.35	1.31
8S9	10,029	1.61	1.94	1.13	1.06	0.69	0.81
8S10	30,222	2.74	4.09	0.95	0.98	1.65	1.58
14S1	21,623	1.74	0.99	1.08	0.93	1.64	1.84
14S2	26,919	1.05	0.87	1.05	1.06	1.59	1.44
14S3	11,022	0.87	0.51	1.12	1.15	0.92	1.21
14S4	23,852	1.67	1.07	1.02	1.02	1.81	2.03
14S5	22,672	1.78	0.97	1.03	0.97	1.72	1.93
14S6	25,247	0.97	0.76	1.08	0.99	1.49	1.35
14S8	58,679	1.43	1.27	1.05	0.96	0.28	0.24
14S9	24,169	0.93	0.72	1.09	0.95	1.42	1.29
Avg.		1.32	1.25	1.08	1.07	1.09	1.17
STD		0.56	0.78	0.15	0.11	0.54	0.55

Table 8. Comparison of different models with literature test data, as obtained in terms of M_n .

Test	M_n (kN·m)	Test/EC3	Test/Kong and Kim	Test/Pucinotti	Test/ KHA-ANN	Test/Multiple Linear Regression	Test/ Genetic Algorithm
8S1	43.6	1.11	1.22	1.14	1.00	1.11	1.11
8S2	44.9	0.93	0.95	0.76	1.03	1.04	1.02
8S3	54.2	1.11	1.22	1.13	1.25	1.38	1.35
8S4	21.7	1.17	1.21	1.09	1.15	0.50	0.69
8S5	43.3	1.02	1.09	1.26	0.99	1.00	0.99
8S6	33.1	1.25	1.37	1.33	1.23	0.84	0.94
8S7	47.4	1.34	1.47	0.75	1.09	1.09	1.08
8S8	50.4	1.87	2.07	0.92	0.95	1.25	1.15
8S9	54.6	1.56	1.67	1.19	0.99	1.30	1.39
8S10	74.7	1.35	1.37	0.70	1.00	1.50	1.55
14S1	83.7	1.08	1.11	1.12	0.93	0.61	0.63
14S2	168.8	0.75	1.12	0.83	1.02	0.80	0.90
14S3	80.9	1.30	1.31	1.29	1.25	1.35	1.30
14S4	101.3	1.03	1.06	1.18	1.00	0.74	0.76
14S5	119.9	1.22	1.57	1.66	1.21	0.90	0.93
14S6	127.4	1.00	1.03	0.88	1.03	0.81	0.91
14S8	186.9	1.045	1.07	0.875	1.04	1.04	1.01
14S9	123.8	0.97	1.00	0.9	1.00	0.79	0.78
Avg.		1.17	1.27	1.05	1.06	1.00	1.03
STD		0.25	0.28	0.24	0.10	0.28	0.25

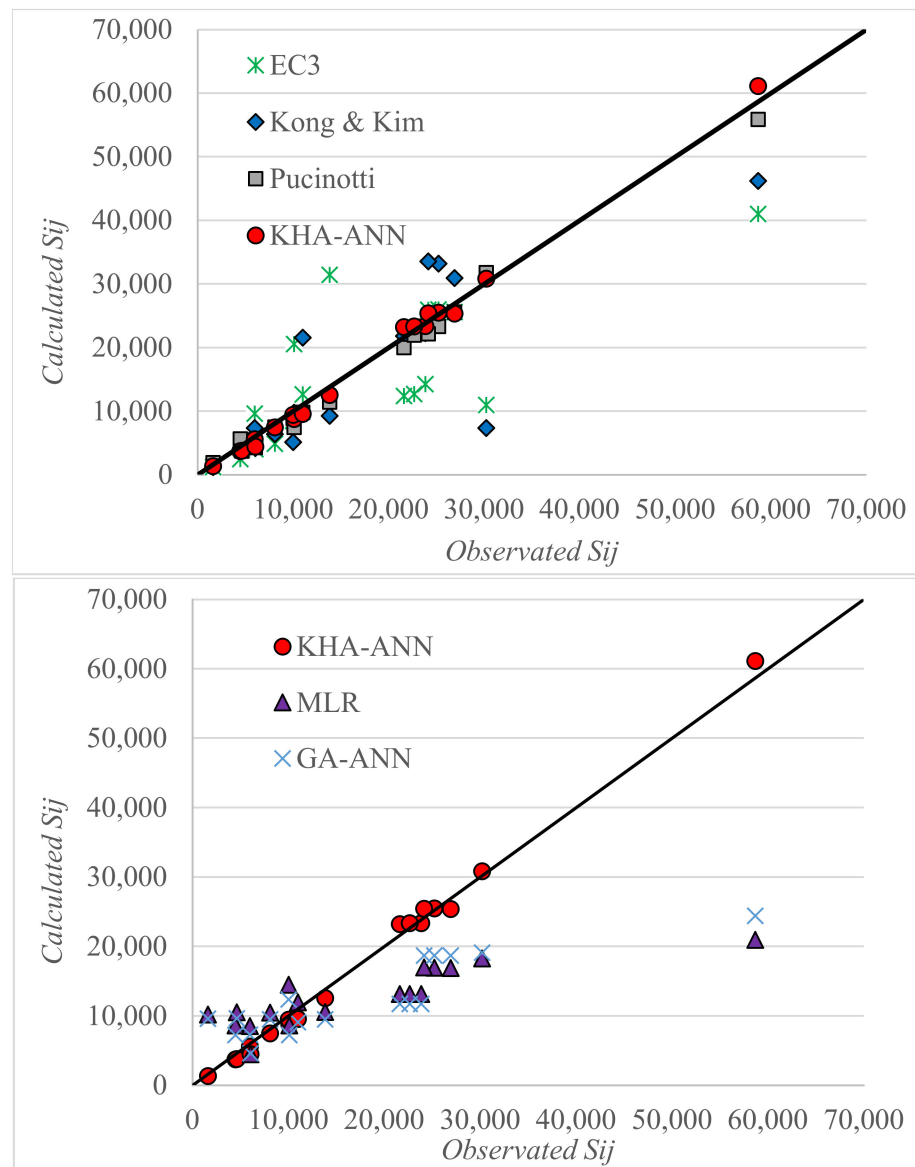


Figure 13. Comparison between experimental and theoretical models for $S_{j,ini}$.

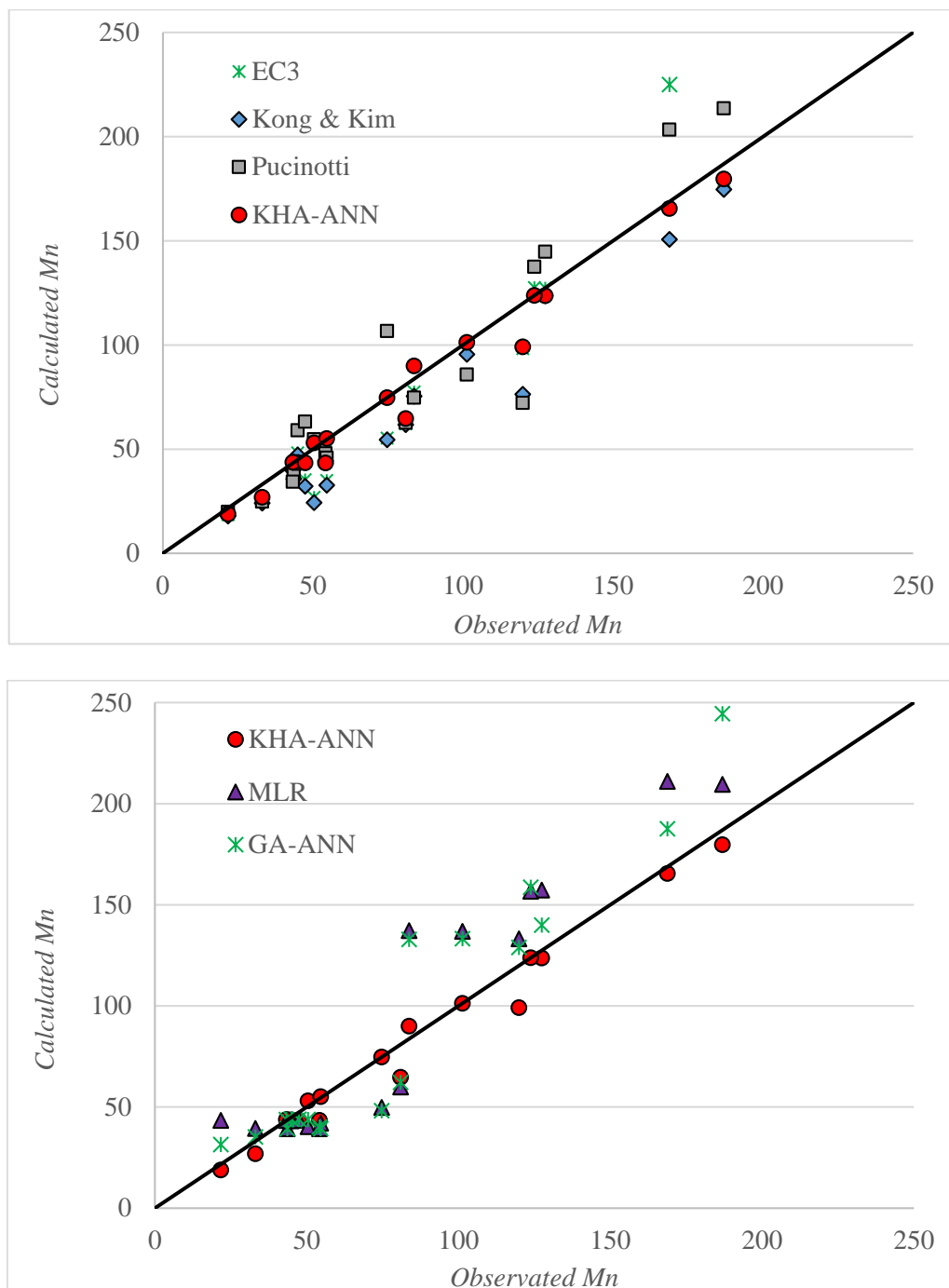


Figure 14. Comparison between experimental and theoretical models for M_n .

The maximum, minimum, and average ratios of the test to theoretical $S_{j,ini}$ and M_n parameters, along with the corresponding coefficient of variation CoV , calculated per the following equation, are provided in Table 9.

$$CoV = \frac{\text{Standard Deviation}}{\text{Average Value}} = \frac{\sqrt{\frac{\sum_{i=1}^n (x_i - \bar{x})^2}{n-1}}}{x} \quad (27)$$

where $x_i = \frac{\text{Experimental } S_{j,ini} \text{ or } M_n}{\text{Theoretical } S_{j,ini} \text{ or } M_n}$; and $\bar{x} = \sum_{i=1}^n \frac{x_i}{n}$.

Table 9. Ratio of actual to predicted $S_{j,ini}$, and M_n parameters for models considered.

Theoretical Models	Minimum	Maximum	Average	$CoV_{test}/CoV_{theoretical}$
$S_{j,ini}/S_{j,ini,theoretical}$				
EC3	0.44	2.74	1.32	1.02
Kong and Kim	0.51	4.09	1.25	0.97
Pucinotti	0.79	1.41	1.08	0.96
Genetic algorithm	0.17	2.03	1.17	0.35
MLR	0.16	1.81	1.11	0.39
KHA-ANN	0.93	1.35	1.07	0.97
$M_n/M_{n,theoretical}$				
EC3	0.75	1.87	1.17	0.77
Kong and Kim	0.95	2.07	1.27	0.85
Pucinotti	0.7	1.66	1.05	0.84
Genetic algorithm	0.63	1.55	1.02	0.87
MLR	0.50	1.50	1.00	0.86
KHA-ANN	0.93	1.25	1.06	0.98

Table 9 indicates that the proposed hybrid KHA-ANN model yields the most reliable results for mechanical properties prediction. The maximum and average ratio of the test to theoretical $S_{j,ini}$ and M_n parameters estimated by the KHA-ANN model was the closest to unity, indicating robust predictive ability. Meanwhile, the minimum value estimated by this model for $S_{j,ini}$ and M_n parameters was equal to 0.93, resulting in accurate yet conservative predictions, which is convenient for design purposes. The results also show that the ratio of the test's coefficient of variation to the theoretical values was estimated to be 0.97 and 0.98 for $S_{j,ini}$ and M_n parameters, respectively, by the KHA-ANN model, indicating its superior accuracy to the other models considered in this study.

Another visual measure that can be taken into account for comparing the performance of the KHA-ANN model against the component-based mechanical model is the Taylor diagram, see Figures 15 and 16. This diagram depicts a graphical illustration of the adequacy of each investigated model, based on the root-mean-square-centered difference, the correlation coefficient, and the standard deviation.

The results proposed in Figures 14 and 15 indicate that the closest prediction for both the $S_{j,ini}$ and M_n input parameters, to the point representing the experimental data in the literature, are provided by the KHA-ANN model developed herein. The component-based model proposed by Pucinotti, as shown, also results in high values of root-mean-square-centered difference and standard deviation, thus further suggesting good accuracy of the formulation over the selected experimental data. Conversely, the same comparative parameters are relatively too low regarding the application of the EC3 model to the selected experimental specimens.

Tables 10 and 11 provide the final weight for both hidden layers by application of the KHA-ANN model. Using the values of weights between different layers of ANN, it is possible to determine and predict the $S_{j,ini}$ and $\frac{M_n}{M_{p,beam}}$.

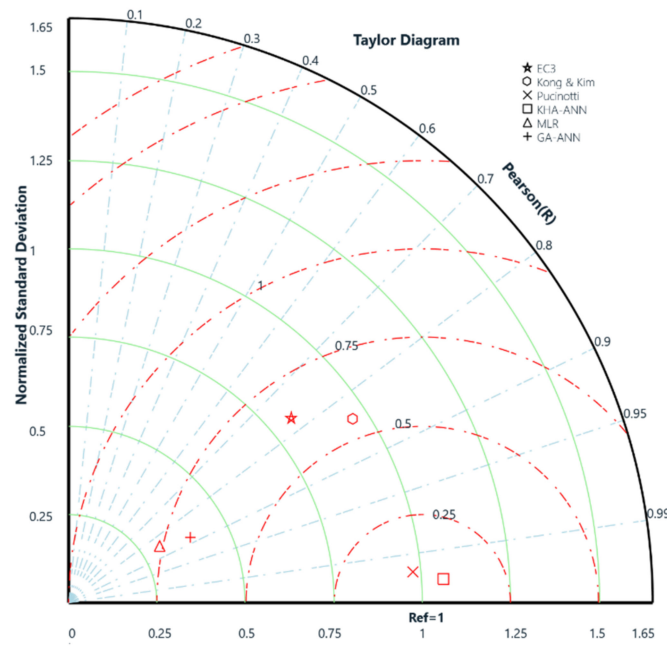


Figure 15. Taylor diagram visualization of model performance, in terms of $S_{j,ini}$ prediction.

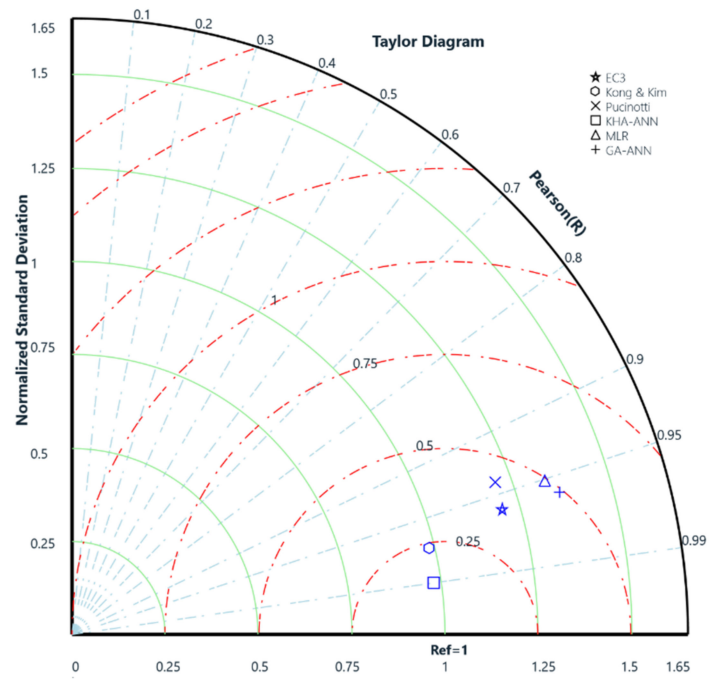


Figure 16. Taylor diagram visualization of model performance, in terms of M_n prediction.

Table 10. Final weights and bias values of the optimum KHA-ANN model for the ratio of M_{in}/M_{pbeam} .

IW						b1	
0.7514	0.0535	0.0958	−0.0792	−0.1804	−0.6325	−0.2747	
0.4097	0.2051	−0.0213	0.0424	0.1579	0.1816	−0.0143	
−0.6575	0.4321	−0.2058	−0.0650	0.3990	−0.2737	0.1995	
0.2339	−0.8016	−0.4855	−0.1924	−0.3408	−0.1798	−0.0717	
−0.1071	0.4356	0.9440	−0.3874	−0.0518	0.2166	0.0639	
−0.0276	0.0805	−0.3331	−0.1355	−0.1292	−0.1902	0.7536	
0.1837	0.1549	−0.3965	0.2715	0.0351	−0.0581	0.1724	
LW1						b2	
0.486836	0.232199	0.178818	0.19609	0.19983	0.204216	−0.0893	0.5233
−0.35536	−0.71724	−0.64976	−0.788	−0.54886	0.606369	−0.1354	0.1026
0.438549	0.307981	−0.07002	0.099073	−0.68334	0.244562	0.2810	0.7008
0.822261	0.257671	−0.2456	0.064399	−0.00797	0.5287	−0.4390	−0.3015
0.638967	0.347942	−0.51478	0.230256	0.122677	0.141804	−0.7414	0.3832
−0.26656	−0.25888	−0.15317	0.300429	0.455593	−0.03802	−0.1338	−0.1351
LW2						b3	
0.9681	−0.6657	−0.7876	−0.2552	−0.6038	−0.0206		−0.3210

IW: weights values for input layer; LW1: weights values for first hidden layer; LW2: weights values for second hidden layer; b1: bias values for first hidden layer; b2: bias values for second hidden layer; b3: bias values for output layer.

Table 11. Final weights and bias values of the optimum KHA-ANN model for $S_{j, ini}$ (kNm/rad).

IW						b1	
0.4909	0.0796	−0.2764	−0.5954	0.0284	−0.2423	−0.0895	
0.4492	−0.0926	−0.1428	0.0302	−0.3488	0.3437	0.1813	
−0.1479	0.0582	−0.2119	−0.2836	0.2420	0.0284	0.4236	
−0.2780	−0.4243	−0.5634	−0.0486	0.1429	−0.4097	0.1867	
−0.1867	−0.1417	0.2382	−0.1349	0.4164	0.5311	−0.3966	
0.3095	0.0664	−0.3421	0.0480	−0.1781	−0.4250	0.0680	
0.0033	−0.1334	−0.4464	0.0177	−0.3164	−0.2103	−0.1803	
LW1						b2	
0.0471	0.3241	0.4336	−0.2665	0.3534	0.2147	−0.3209	−0.0945
−0.5778	−0.1768	−0.1420	−0.0004	−0.5863	0.0144	0.3295	0.1550
0.3186	−0.3091	0.0413	−0.2326	0.1294	−0.3266	0.2789	0.1893
0.5598	0.2860	−0.5133	−0.1338	0.0662	0.3885	−0.0985	−0.2359
−0.0901	0.5717	−0.3920	−0.1306	0.3884	−0.0880	0.1531	0.0450
0.3889	0.4165	−0.4297	−0.0532	0.2369	0.5079	−0.0817	0.4104
LW2						b3	
0.9681	−0.6657	−0.7876	−0.2552	−0.6038	−0.0206		−0.3210

IW: weights values for input layer; LW1: weights values for first hidden layer; LW2: weights values for second hidden layer; b1: bias values for first hidden layer; b2: bias values for second hidden layer; b3: bias values for output layer.

6. Comparison and Discussion of the Mechanical and Informational Approaches

The plastic response of different components and their interactions are recognized as the main challenge of modeling the behavior of bolted beam-to-column connections. It is possible to represent the complex behavior of bolted connections, i.e., slippage, residual stress, and friction, using a detailed finite element method; however, integrating such an approach into the analysis and design process of a real structure becomes time-consuming and impractical. An informational model using ANNs and component-based mechanical models was developed in this research to represent the behavior of steel bolted beam-to-column connections. The features of these two distinct methods are discussed herein.

The constitutive contacts of all the components in bolted connections are set up through geometric and material properties using the principle of virtual forces. The efficiency of this approach depends on the accuracy of the relationships of the constitutive component and the number of components. By defining an acceptable number of components and subsequently conceptualizing the physical behavior as analytical equations, applying the mechanical model to different connection configurations is possible. Nevertheless, conceptualization typically resulted in equations that exclude several essential features of physical behavior. To properly simulate the mechanical properties of bolted angle connections, the main challenge is recognized as due to slippage, which affects the initial and hardening stiffness. Slippage is a possibility of the connection deforming before it starts to transmit forces. This has nothing to do with the capacity of the connection, only with its rigidity. Screwed connections with long holes (without pre-tensioning) are the best example of slippage.

Unlike the conventional mechanical modeling process that involves conceptualization from the observed behavior to the mathematical equations, in the informational base method, the information about essential behavior is extracted from the available experimental test data and processed using ANNs. Accordingly, there is no need for pre-defined mathematical equations, unlike the component-based mechanical method. The main advantage of the proposed methodology is that the ANN-based model can learn the complex $M-\theta$ relationship of the connection's components due to frictional slippage, buckling, slacking of fastened bolts, and fracture as the yielding of materials. However, the ANN model of the bolted connection is limited to only estimating the global response that includes the contribution of all components. Using this method, it is impossible to represent the contribution of individual components; therefore, it does not offer an insight into the underlying mechanics. This poses difficulties in applications and extensions to other beam-to-column connection configurations and material properties [60]. To improve network prediction quality, it is suggested that the ANN interpolates rather than extrapolates from a particular training set. Meanwhile, for training the ANN, it is recommended that all possible mixtures of design variables in practice be considered.

The results of observational and computational data for both $S_{j,ini}$ and $M_n/M_{p,beam}$ outputs are shown in Figure 17 for all 77 specimens. Figure 17 indicates that samples having constant design variables (shown with green circles) caused an error in output results.

Overall, given that the performance and behavior of steel connections are non-linear, the application of ANNs optimized with metaheuristic algorithms can be effective. Moreover, the combination of ANNs and component-based mechanical models can be employed for beam-to-column connections with different configurations, so the advantages of the two methods are implemented, and their disadvantages are accounted for.

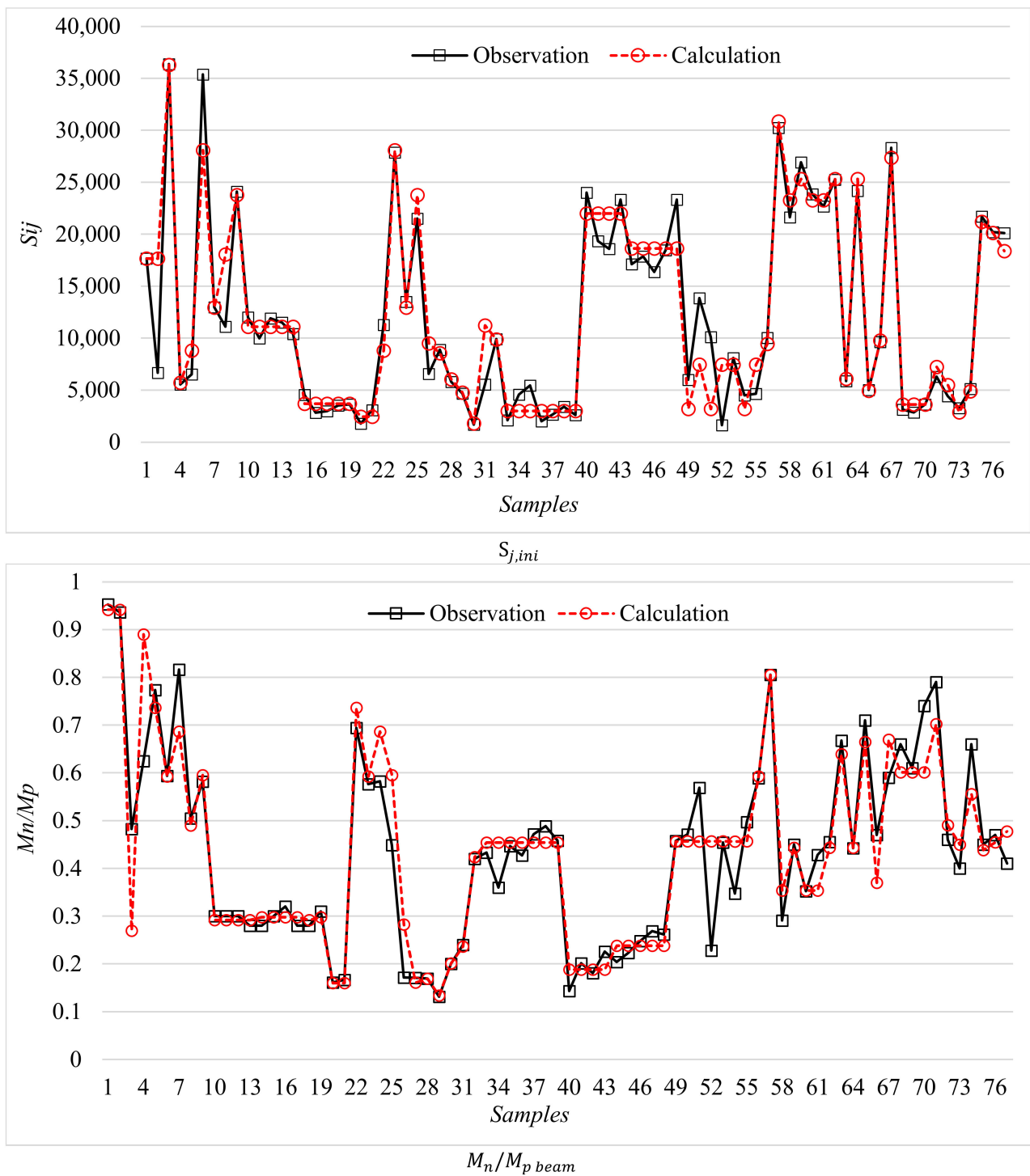


Figure 17. The difference between observational and computational results for $S_{j,ini}$ and $M_n/M_{p,beam}$.

7. Concluding Remarks

In this research, three different mechanical models have been presented, and their capacities for estimating the mechanical properties of top- and seat-angle connections with double-web angles were examined. In the second phase of research, a novel hybrid krill herd algorithm-artificial neural network (KHA-ANN) model was proposed to acquire an informational model from the available experimental test dataset. The following conclusions have been drawn based on the results of this study:

- I. The proposed simplified mechanical models have sufficient accuracy in estimating the mechanical properties of bolted beam-to-column connections. This method's main challenge is defining a sufficient number of components and conceptualization from physical behavior to analytical equations. The component-based mechanical models can be applied to different connection configurations, provided that the fundamental components with their non-linear response are accurately identified.
- II. The novel hybrid KHA-ANN model established an excellent agreement with the experimental database. The results suggest that the informational model may be a reliable alternative to the mechanical model for estimating the mechanical properties of bolted beam-to-column connections. Although this method has the valuable characteristic of being user-friendly, it was limited to only presenting the global response including the contribution of all components. Therefore, it does not offer an insight into the underlying mechanisms of individual components.
- III. The results of the ANN model optimized by the krill herd algorithm acknowledged that this algorithm is quite successful in finding the optimal point of functions. This model has good potential compared to multilinear regression and genetic algorithm models where AAE, VAF, and EF statistical coefficients have higher values, indicating a lower error of this model. The maximum and average ratios of the test to theoretical $S_{j,ini}$ and M_n parameters estimated by the KHA-ANN model were the closest to unity, indicating robust predictive capability.

Author Contributions: This research paper results from a joint collaboration of all the involved authors. All authors contributed to the paper drafting and review, I.F., M.N., R.P. and M.H.B. All authors have read and agreed to the published version of the manuscript.

Funding: This work was supported by funding from the Federal State Autonomous Educational Institution of Higher Education South Ural State University (National Research University).

Institutional Review Board Statement: The study did not require ethical approval.

Informed Consent Statement: Not applicable.

Data Availability Statement: Data sharing not applicable.

Conflicts of Interest: The authors declare no conflict of interest.

References

1. Alwanas, A.A.H.; Al-Musawi, A.A.; Salih, S.Q.; Tao, H.; Ali, M.; Yaseen, Z.M. Load-carrying capacity and mode failure simulation of beam-column joint connection: Application of self-tuning machine learning model. *Eng. Struct.* **2019**, *194*, 220–229. [[CrossRef](#)]
2. Lian, M.; Zhang, H.; Cheng, Q.; Su, M. Finite element analysis for the seismic performance of steel frame-tube structures with replaceable shear links. *Steel Compos. Struct.* **2019**, *30*, 365–382. [[CrossRef](#)]
3. Bayat, M.; Zahrai, S.M. Seismic performance of mid-rise steel frames with semi-rigid connections having different moment capacity. *Steel Compos. Struct.* **2017**, *25*, 1–17. [[CrossRef](#)]
4. Lian, M.; Cheng, Q.; Zhang, H.; Su, M. Numerical study of the seismic behavior of steel frame-tube structures with bolted web-connected replaceable shear links. *Steel Compos. Struct.* **2020**, *35*, 305–325. [[CrossRef](#)]
5. Wang, J.; Uy, B.; Li, D.; Song, Y. Progressive collapse analysis of stainless steel composite frames with beam-to-column endplate connections. *Steel Compos. Struct.* **2020**, *36*, 427–446. [[CrossRef](#)]
6. Pnevmatikos, N.; Konstandakopoulou, F.; Blachowski, B.; Papavasileiou, G.; Broukos, P. Multifractal analysis and wavelet leaders for structural damage detection of structures subjected to earthquake excitation. *Soil Dyn. Earthq. Eng.* **2020**, *139*, 106328. [[CrossRef](#)]
7. En, B. *Eurocode 3: Design of Steel Structures—Part 1–8: Design of Joints*; British Standards Institution: London, UK, 2005; pp. 1–8.
8. Nakashima, M.; Inoue, K.; Tada, M. Classification of damage to steel buildings observed in the 1995 Hyogoken-Nanbu earthquake. *Eng. Struct.* **1998**, *20*, 271–281. [[CrossRef](#)]
9. Lopez, A.; Puente, I.; Aizpurua, H. Experimental and analytical studies on the rotational stiffness of joints for single-layer structures. *Eng. Struct.* **2011**, *33*, 731–737. [[CrossRef](#)]
10. Elghazouli, A.; Málaga-Chuquitaype, C.; Castro, J.; Orton, A. Experimental monotonic and cyclic behaviour of blind-bolted angle connections. *Eng. Struct.* **2009**, *31*, 2540–2553. [[CrossRef](#)]

11. Guan, D.; Yang, S.; Jia, L.-J.; Guo, Z. Development of miniature bar-type structural fuses with cold formed bolted connections. *Steel Compos. Struct.* **2020**, *34*, 53–73. [[CrossRef](#)]
12. Wang, J.; Wang, J.; Wang, H. Seismic behavior of blind bolted CFST frames with semi-rigid connections. In *Structures*; Elsevier: Amsterdam, The Netherlands, 2017; pp. 91–104.
13. Abolmaali, A.; Kukreti, A.; Motahari, A.; Ghassemieh, M. Energy dissipation characteristics of semi-rigid connections. *J. Constr. Steel Res.* **2009**, *65*, 1187–1197. [[CrossRef](#)]
14. Oskouei, A.V.; Fard, S.S.; Aksogan, O. Using genetic algorithm for the optimization of seismic behavior of steel planar frames with semi-rigid connections. *Struct. Multidiscip. Optim.* **2012**, *45*, 287–302. [[CrossRef](#)]
15. Pirmoz, A.; Liu, M.M. Direct displacement-based seismic design of semi-rigid steel frames. *J. Constr. Steel Res.* **2017**, *128*, 201–209. [[CrossRef](#)]
16. Hassan, E.M.; Admuthe, S.; Mahmoud, H. Response of semi-rigid steel frames to sequential earthquakes. *J. Constr. Steel Res.* **2020**, *173*, 106272. [[CrossRef](#)]
17. Abdollahzadeh, G.; Shabaniyan, S.M. Experimental and numerical analysis of beam to column joints in steel structures. *Front. Struct. Civ. Eng.* **2018**, *12*, 642–661. [[CrossRef](#)]
18. He, M.; Luo, J.; Tao, D.; Li, Z.; Sun, Y.; He, G. Rotational behavior of bolted glulam beam-to-column connections with knee brace. *Eng. Struct.* **2020**, *207*, 110251. [[CrossRef](#)]
19. Sadeghi, S.N.; Heidarpour, A.; Zhao, X.-L.; Al-Mahaidi, R. A component-based model for innovative prefabricated beam-to-hybrid tubular column connections. *Thin Walled Struct.* **2018**, *132*, 265–275. [[CrossRef](#)]
20. Abdollahzadeh, G.; Shabaniyan, S.M.; Tavakol, A. Experimental and numerical evaluation of rigid column to baseplate connection under cyclic loading. *Struct. Des. Tall Spec. Build.* **2019**, *28*, e1596. [[CrossRef](#)]
21. Özkılıç, Y.O. A new replaceable fuse for moment resisting frames: Replaceable bolted reduced beam section connections. *Steel Compos. Struct.* **2020**, *35*, 353–370. [[CrossRef](#)]
22. Blachowski, B.; Pnevmatikos, N. Neural network based vibration control of seismically excited civil structures. *Period. Polytech. Civ. Eng.* **2018**, *62*, 620–628. [[CrossRef](#)]
23. Chen, W.-F.; Kishi, N. Semirigid steel beam-to-column connections: Data base and modeling. *J. Struct. Eng.* **1989**, *115*, 105–119. [[CrossRef](#)]
24. Wales, M.W.; Rossow, E.C. Coupled moment-axial force behavior in bolted joints. *J. Struct. Eng.* **1983**, *109*, 1250–1266. [[CrossRef](#)]
25. Tschemmerneegg, F.; Humer, C. The design of structural steel frames under consideration of the nonlinear behaviour of joints. *J. Constr. Steel Res.* **1988**, *11*, 73–103. [[CrossRef](#)]
26. Madas, P.J.; Elnashai, A.S. A component-based model for beam-column connections. *Proc. Tenth World Conf. Earthq. Eng.* **1992**, *8*, 4495–4499.
27. De Stefano, M.; De Luca, A.; Astaneh-Asl, A. Modeling of cyclic moment-rotation response of double-angle connections. *J. Struct. Eng.* **1994**, *120*, 212–229. [[CrossRef](#)]
28. Shen, J.; Astaneh-Asl, A. Hysteresis model of bolted-angle connections. *J. Constr. Steel Res.* **2000**, *54*, 317–343. [[CrossRef](#)]
29. Díaz, C.; Victoria, M.; Querin, O.M.; Martí, P. FE model of three-dimensional steel beam-to-column bolted extended end-plate joint. *Int. J. Steel Struct.* **2018**, *18*, 843–867. [[CrossRef](#)]
30. Shabaniyan, S.M.; Abdollahzadeh, G.; Davoodi, M. Evaluation of the moment–rotation curve of steel beam-to-column joints with flange-plate. *Asian J. Civ. Eng.* **2019**, *21*, 517–531. [[CrossRef](#)]
31. Soleimani, E.; Behnamfar, F. New moment-rotation equation for welded steel beam-to-column connections. *Int. J. Steel Struct.* **2017**, *17*, 389–411. [[CrossRef](#)]
32. Xing, Y.; Zhao, Y.; Guo, Q.; Jiao, J.-F.; Chen, Q.-W.; Fu, B.-Z. Static behavior of bolt connected steel-concrete composite beam without post-cast zone. *Steel Compos. Struct.* **2021**, *38*, 365. [[CrossRef](#)]
33. Kong, Z.; Kim, S.-E. Moment-rotation behavior of top-and seat-angle connections with double web angles. *J. Constr. Steel Res.* **2017**, *128*, 428–439. [[CrossRef](#)]
34. Pucinotti, R. Top-and-seat and web angle connections: Prediction via mechanical model. *J. Constr. Steel Res.* **2001**, *57*, 663–696. [[CrossRef](#)]
35. Azizinamini, A.; Bradburn, J.; Radziminski, J. Initial stiffness of semi-rigid steel beam-to-column connections. *J. Constr. Steel Res.* **1987**, *8*, 71–90. [[CrossRef](#)]
36. Weynand, K.; Huter, M.; Kirby, P.; Simões da Silva, L.; Cruz, P. SERICON—Databank on Joints in Building Frames. In Proceedings of the 1st COST C1 Workshop, Strasbourg, France, 28–30 October 1992.
37. Kishi, N.; Chen, W.-F. *Data Base of Steel Beam-to-Column Connections*; Structural Engineering Area, School of Civil Engineering, Purdue University: West Lafayette, IN, USA, 1986.
38. Málaga-Chuquitaype, C.; Elghazouli, A. Component-based mechanical models for blind-bolted angle connections. *Eng. Struct.* **2010**, *32*, 3048–3067. [[CrossRef](#)]
39. Hasan, M.J.; Ashraf, M.; Uy, B. Moment-rotation behaviour of top-seat angle bolted connections produced from austenitic stainless steel. *J. Constr. Steel Res.* **2017**, *136*, 149–161. [[CrossRef](#)]
40. Ma, L.; Bocchini, P. Hysteretic Model of Single-Bolted Angle Connections for Lattice Steel Towers. *J. Eng. Mech.* **2019**, *145*, 04019052. [[CrossRef](#)]

41. Anwar, G.A.; Dinu, F.; Ahmed, M. Numerical Study on Ultimate Deformation and Resistance Capacity of Bolted T-Stub Connection. *Int. J. Steel Struct.* **2019**, *19*, 970–977. [[CrossRef](#)]
42. Hantouche, E.G.; Sleiman, S.A. Response of double angle and shear endplate connections at elevated temperatures. *Int. J. Steel Struct.* **2016**, *16*, 489–504. [[CrossRef](#)]
43. Kishi, N.; Chen, W.-F. Moment-rotation relations of semirigid connections with angles. *J. Struct. Eng.* **1990**, *116*, 1813–1834. [[CrossRef](#)]
44. Pucinotti, R. Cyclic mechanical model of semirigid top and seat and double web angle connections. *Steel Compos. Struct.* **2006**, *6*, 139–157. [[CrossRef](#)]
45. Ghaboussi, J.; Garrett, J., Jr.; Wu, X. Knowledge-based modeling of material behavior with neural networks. *J. Eng. Mech.* **1991**, *117*, 132–153. [[CrossRef](#)]
46. Ghaboussi, J.; Sidarta, D. New nested adaptive neural networks (NANN) for constitutive modeling. *Comput. Geotech.* **1998**, *22*, 29–52. [[CrossRef](#)]
47. Gawin, D.; Lefik, M.; Schrefler, B. ANN approach to sorption hysteresis within a coupled hygro-thermo-mechanical FE analysis. *Int. J. Numer. Methods Eng.* **2001**, *50*, 299–323. [[CrossRef](#)]
48. Abdollahzadeh, G.; Hashemi, S.M.; Tavakoli, H.; Rahami, H. Determination of hysteretic behavior of steel end-plate beam-to-column connection with mechanical and neural network modeling. *Arab. J. Sci. Eng.* **2014**, *39*, 7661–7671. [[CrossRef](#)]
49. Shah, S.; Sulong, N.R.; El-Shafie, A. New approach for developing soft computational prediction models for moment and rotation of boltless steel connections. *Thin Walled Struct.* **2018**, *133*, 206–215. [[CrossRef](#)]
50. Stavroulakis, G.; Avdelas, A.; Abdalla, K.; Panagiotopoulos, P. A neural network approach to the modelling, calculation and identification of semi-rigid connections in steel structures. *J. Constr. Steel Res.* **1997**, *44*, 91–105. [[CrossRef](#)]
51. Cao, Y.; Wakil, K.; Alyousef, R.; Jermsittiparsert, K.; Ho, L.S.; Alabduljabbar, H.; Alaskar, A.; Alrshoudi, F.; Mohamed, A.M. Application of extreme learning machine in behavior of beam to column connections. In *Structures*; Elsevier: Amsterdam, The Netherlands, 2020; pp. 861–867.
52. Iman Faridmehr, M.N. Raffaele Pucinotti and Chiara Bedon. Application of Component-Based Mechanical Models and Artificial Intelligence to Bolted Beam-to-Column Connections. *Appl. Sci.* **2021**, *11*, 2297. [[CrossRef](#)]
53. Hasanzade-Inallu, A.; Zarfam, P.; Nikoo, M. Modified imperialist competitive algorithm-based neural network to determine shear strength of concrete beams reinforced with FRP. *J. Cent. South Univ.* **2019**, *26*, 3156–3174. [[CrossRef](#)]
54. Kotsovou, G.M.; Cotsovos, D.M.; Lagaros, N.D. Assessment of RC exterior beam-column Joints based on artificial neural networks and other methods. *Eng. Struct.* **2017**, *144*, 1–18. [[CrossRef](#)]
55. DmitriyTarkhov, A. 3-Methods for the selection of parameters and structure of the neural network model. In *Semi-Empirical Neural Network Modeling and Digital Twins Development*; Elsevier: Amsterdam, The Netherlands, 2020; pp. 73–103. [[CrossRef](#)]
56. Asteris, P.G.; Nozhati, S.; Nikoo, M.; Cavaleri, L.; Nikoo, M. Krill herd algorithm-based neural network in structural seismic reliability evaluation. *Mech. Adv. Mater. Struct.* **2019**, *26*, 1146–1153. [[CrossRef](#)]
57. Bolaji, A.L.a.; Al-Betar, M.A.; Awadallah, M.A.; Khader, A.T.; Abualigah, L.M. A comprehensive review: Krill Herd algorithm (KH) and its applications. *Appl. Soft Comput.* **2016**, *49*, 437–446. [[CrossRef](#)]
58. Faridmehr, I.; Bedon, C.; Huseien, G.F.; Nikoo, M.; Baghban, M.H. Assessment of Mechanical Properties and Structural Morphology of Alkali-Activated Mortars with Industrial Waste Materials. *Sustainability* **2021**, *13*, 2062. [[CrossRef](#)]
59. Nikoo, M.; Torabian Moghadam, F.; Sadowski, Ł. Prediction of concrete compressive strength by evolutionary artificial neural networks. *Adv. Mater. Sci. Eng.* **2015**, *2015*, 849126. [[CrossRef](#)]
60. Kim, J.; Ghaboussi, J.; Elnashai, A.S. Mechanical and informational modeling of steel beam-to-column connections. *Eng. Struct.* **2010**, *32*, 449–458. [[CrossRef](#)]